IEEE Access
Multidisciplinary | Rapid Review | Open Access Journal

Received March 28, 2020, accepted April 15, 2020, date of publication April 20, 2020, date of current version May 5, 2020.

Digital Object Identifier 10.1109/ACCESS.2020.2988769

A Novel Amplitude Modulation Architecture via Time-Varying Programmable Metasurface for Wireless Communication Systems

LIWEN CHEN[1], (Member, IEEE), QING WENG[1], JING CHEN[1], AND JIAN-FENG GU[2,3], (Member, IEEE)

[1]Key Laboratory of Automotive Electronics and Electric Drive Technology, Fujian University of Technology, Fuzhou 350108, China
[2]Moonshot Health Inc., Montréal, QC H4E 1A2, Canada
[3]Department of Electrical Engineering, Polytechnique de Montréal, Montréal, QC H3T 1J4, Canada

Corresponding author: Liwen Chen (chenlw2002@whu.edu.cn)

This work was supported in part by the CSC, Fujian Science and Technology Department, under Grant 2018H01010223, in part by the Quanhzou Science and Technology Bureau under Grant 2017G012, in part by the Fujian University of Technology under Grant GY-Z17011, and in part by the Department of Education of Fujian Province under Grant JT180339.

ABSTRACT Different from the traditional wireless communication systems, where both amplitude and phase components are used to provide a form of modulation, almost all of space time-modulated matesurface (MS) currently reported are modulated by phase components. In this paper we propose a new architecture of time-varying modulated MS based on two features. First, inspired by the idea of beamforming-like techniques that different digital sequences are added to the MS, in this way, the amplitude can be changed rapidly for modulation by holding the constant phase. Here, a pentagonal array-based MS is designed to achieve amplitude modulation (AM) by the use of on-off field programming gate array (FPGA) hardware. Second, a quasi-optical measurable scheme in the near-filed is used to show the phenomena and detect the measurements. To verify the ideas mentioned above, the simulations and measurements are carried out.

INDEX TERMS Time-varying programmable MS, amplitude modulation, FPGA, quasi-optical, pentagonal array.

I. INTRODUCTION

Thanks to unique features of a space-time modulated MS with the two-dimensional equivalent artificial engineered structure, recently, the MS has been paid more attention to the potential applications in the electromagnetic (EM) fields, such as optical antireflection coating [1], reconfigurable antenna [2], negative refraction [3], meta-hologram [4], [5] and super-resolution imaging [6], just to name a few.

Since EM waves are propagated in a wireless environment, they are difficult for us to be controlled. Fortunately, a class of planar metamaterials called MSs are invented to control the impinging EM waves by a way of software-defined scheme. In this way, EM waves can be effectively engineered, such as steering toward any desired direction, full absorption and polarization manipulation. The authors of [7] used digital MS to control phase shifts where the phase has a 180 ° difference to express a 1-bit digital provided that the amplitude is almost constant. In [8] and [9] the authors proposed ways to generate temporal harmonics to control the propagation direction and harmonic power distribution by time-modulated MS. It also can be considered as a frequency selective surface for circuit analysis [10], [11]. Transmission-Line structure is used as a leaky-wave antenna with tunable radiation angle and beamwidth [12]. Birefringent operations can be used to convert linear polarization into circular polarization [13].

As known to us that signal absorption, reflections, refractions, and diffractions induced by physical objects as well as free space path loss will highly reduce the quality of wireless communication systems. The use of the MS mitigates the path loss by enforcing the lens effect and avoiding the ambient dispersal of energy and non-line-of-sight (NLOS) effects as well, eventually extending the effective communication range [14].

In addition, the authors of [15] claimed that graded MS by transverse temporal modulation can improve rapid communication. Hybrid graphene MS structures presented in [16]

The associate editor coordinating the review of this manuscript and approving it for publication was Qammer Hussain Abbasi.

can optimize the efficient terahertz modulation. Broadband MS is introduced in [17] to change amplitude and phase simultaneously in the space domain. The work of [18] was to invent high-resolution holograms, which has been developed for storing and recovering the amplitude and phase of light scattered by objects. The authors of [19] introduced an impedance-based amplitude synthesis method by the use of aperture field distribution for space domain.

It is also known to us that the MS can control the propagation direction and harmonic power distribution [20]. According to the recent research on the form of modulation of the MS, the phase modulation (PM) is used with the constant amplitude [21], [22]. In [23] the authors proposed a MS with split-ring resonators (SRR) and inserted chip resisters for absorption, which can used in energy harvesting and stealth fields. Later the author of [24] presented a coding MS is composed of SRR and inserted chip resisters for generating AM radiation patterns.

Different from the phase modulated MS [25] and non-continuous AM modulation, in this paper, we introduce a new programmable MS architecture that different digital sequences controlled by FPGA is added to the MS, where the amplitude is changed significantly while the phase is almost constant. In addition, the proposed architecture enjoys some good features such as low hardware cost, low energy consumption and simple structure. Therefore, we can modulate the changed amplitude for wireless communication applications.

The rest of the paper is organized as follows. Section II provides a concept of space-time programmable MS, including fundamental principle, MS structure design and simulation. Section III describes the design and fabrication scheme of our proposed digital MS, including prototype setup, transmitter design and some experimental results. Finally, the conclusion is given in Section IV.

II. THEORY AND DESIGN

A. TIME-VARYING MS DESIGN

Rapid development in wireless communications systems has demanded wider bandwidth, higher capacity and lower power consumption to support the practical requirements, which puts forward new challenges for the traditional zero intermediate frequency (zero-IF) or superheterodyne architecture. For example, the time-varying based direct antenna modulation technique can generate modulated RF signals directly, but it can only be exploited for few ineffective modulation schemes such as on-off keying (OOK) [26] and frequency shift keying (FSK) [27]. The paper proposes a MS structure, which is a flexible hardware architecture to deal with the shortcomings for future wireless communication systems.

The transmitter of our proposed architecture is shown in the left part of Figure 1. It consists of the programmable MS, the control circuit board, software design radio and lens. From the figure, a source from signal generator is provided and the related incident wave from a feed antenna impinges on the

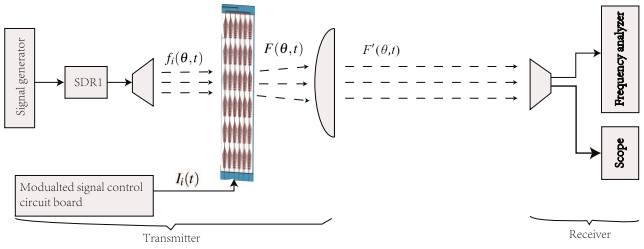

FIGURE 1. MS wireless communication architecture.

programmable MS. The incident wave $f_i(\theta, t)$ is a single-tone carrier signal as the carrier signal in our metasurface-based wireless communication system. The programmable wave $F(\theta, t)$ of the MS contains the modulated information $I_i(t)$ of the carrier frequency of the incident wave and $F\prime(\theta, t)$ depicts the programmable wave that passing through a think lens, that bulges outward on one side and is flat on the other. The main parts of the receiver are the receiving antenna, scope and frequency analyzer shown in the right part of Figure 1. RF signal is captured by the scope or the frequency analyzer.

B. SPACE-TIME CONCEPT AND DESCRIPTION

The space-time digital MS can be configured as a linear array with N elements. A periodic time-domain continuous wave (CW) impinging in the MS can be described as a linear pulse function

$$F(\theta, t) = \sum_{m=-\infty}^{\infty} \sum_{i=1}^{N} A_i a_{mi} e^{j2\pi(f+mf_0)t} \exp\left(j\frac{2\pi}{\lambda_c} d_i \sin\theta\right) \tag{1}$$

where A_i is the amplitude of the $i-th$ element. λ_c and d_i are the wavelength of the CW signal and the distance between the $i-th$ element and the reference element. The elevation angle is θ and f is the operating frequency of the CW signal, f_0 is the switching frequency given by $f_o = 1/T_0$ and T_0 is the switching period. For simplicity, it is assumed $nT_0 \leq t_{ion} \leq t_{ioff} \leq (n+1)T_0$, where t_{ion} and t_{ioff} denote periodically switched on and off of the $i-th$ element, respectively. In addition, the periodic voltage changing of $i-th$ element is written as

$$I_i(t) = \begin{cases} 1, & nT_0 + t_{ion} \leq t < nT_0 + t_{ioff} \\ 0, & \text{elsewhere} \end{cases} \tag{2}$$

Here, we consider T_{ion} and T_{ioff} as the rising and the falling edge trigger shown in Figure 2, respectively. The period of the pulse-width modulation is T_0.

The rising edge trigger of each element is defined by $T_{ion} = nT_0 + t_{ion}$, and the falling edge trigger of each element is $T_{ioff} = nT_0 + t_{ioff}$. The Fourier expansion of $I_i(t)$ can be expressed as

$$I_i(t) = \sum_{m=-\infty}^{\infty} b_{mi} \exp\left(j2\pi m f_0 t\right), \tag{3}$$

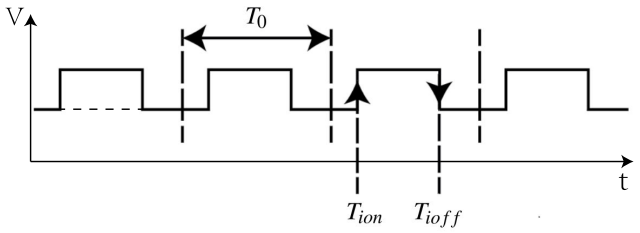

FIGURE 2. A PWM sequence with respect to time generated by FPGA. T_{ion}, T_{ioff} and T_0 denote the rising and falling edge and the switching cycle, respectively.

and b_{mi} is the coefficients of Fourier series can be written by

$$b_{mi} = \frac{1}{T_0}\int_0^{T_0} I_i(t)\exp\left(-j2\pi m f_0 t\right)dt \tag{4}$$

$f_o = 1/T_0$ is the switching frequency and a_{mi} is the coefficients of $F(\theta, t)$ as

$$\begin{aligned} a_{mi} &= \sum_{i=0}^{N-1} b_{mi} = \sum_{i=0}^{N-1}\frac{1}{T_0}\int_{iT_0+T_{ion}}^{iT_0+T_{ioff}} e^{-j2\pi m f_0 t}dt \\ &= \sum_{i=0}^{N-1} f_0\left(T_{ioff}-T_{ion}\right)\mathrm{sinc}\left\{\pi m f_0\left(T_{ioff}-T_{ion}\right)\right\}e^{-j\pi mi} \end{aligned} \tag{5}$$

The amplitude and phase of each element can be represented as A_i^m and φ_i^m at different harmonic frequencies.

$$A_i^m = \left|\sum_{i=0}^{N-1} A_i f_0\left(T_{ioff}-T_{ion}\right)\mathrm{sinc}\left\{\pi m f_0\left(T_{ioff}-T_{ion}\right)\right\}e^{-j\pi mi}\right| \tag{6}$$

$$\varphi_i^m = \arg\left\{\sum_{i=0}^{N-1} A_i f_0\left(T_{ioff}-T_{ion}\right)\mathrm{sinc}\left\{\pi m f_0\left(T_{ioff}-T_{ion}\right)\right\}e^{-j\pi mi}\right\} \tag{7}$$

From the above theoretical analysis, we can observe that the harmonic beam steering has the property of time shift in the Fourier transform domain, so we can control the scattering patterns at any harmonic frequencies accuracy. From Eq. (6) and Eq. (7), the equivalent AM and PM can be verified, 1-bit space-time digital MS is designed, where the signal can be steered to the desired direction when the beam is set at the central frequency.

C. MS STRUCTURE DESIGN

As illustrated in Fig 3, a pentagonal spiral structure with a pin diode has been added to the MS structure. For biasing the pin diode, the resonant response is perturbed and it will appear two different half-wave resonant structures. The current flows from up to down into the center ground when the pin diode is short in Fig 3. From the Eqs. (6) and (7), we observe

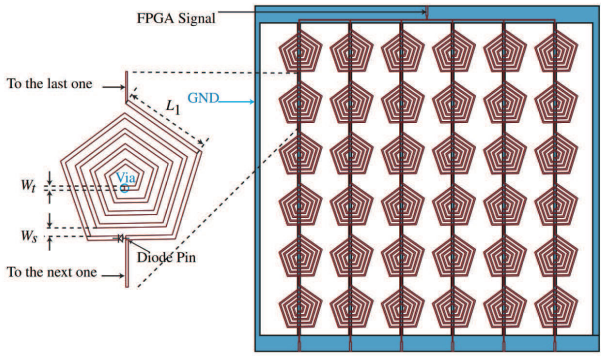

FIGURE 3. Layout of the MS prototype. The whole MS is shown on the right side and the details of each element are shown on the left side. On the left side is the unit cell of the MS. The related parameters are set up Wt = 0.5 mm, Ws = 1 mm and L1 = 11.176 mm.

that the number of elements N, bias-voltage A_i, resonance frequency f_0, and high level $T_{ihigh} = T_{ioff} - T_{ion}$ in each period can impact the amplitude and phase components. In the figure, the single element has been extended to a cycled $6 * 6$ structure. In the case, the output signal controlled by FPGA hardware [28] is a form of the pulse width modulation (PWM) and the current is flow from above to top elements separated to 6 parallel columns, and through each element to the bottom elements.

As shown in Fig 3, each column consisting six pentagon spiral elements is connected to power biased lines with a width Wt 0.5 mm and shares a common control voltage. The distance Ws between the adjacent lines is 1 mm and the first length $L1$ of the pentagonal spiral is 11.176 mm. A diode pin is employed to connect the pentagon spiral element with ground (GND) biased lines and these lines connect the bottom GNDs through a via. All the GND is drawn as blue color in the picture. As the pin diode is on (or off) with a biasing voltage of 2.5 V (or 0 V), the corresponding digital status is "1" (or "0").

D. SIMULATION AND ANALYSIS

The local information can be expressed as a voltage changing sequence, so a FPGA hardware is exploited to generate a PWM signal, the duty cycle of the PWM can be defined as

$$p = \frac{T_{ioff} - T_{ion}}{T_0} \tag{8}$$

Hence, we change the duty cycle p under the same voltage in the simulation environment. In Fig 4, the fixed parameters of the system are: input power (0.01 mW), incident angel (0 degree), and the blue line denoting the bias voltage (2.5 V), respectively. The red line is the output result after carrier mixed with the local information, which can be observed in right part of Fig 4 and Fig 5. When the duty cycle is 50 %, the result is a 50 % amplitude modulated envelope. Changing the duty cycle to 75 % and the 75 % amplitude modulated envelope is achieved in Fig 5. The simulation result shows us that the information transmission can be realized through

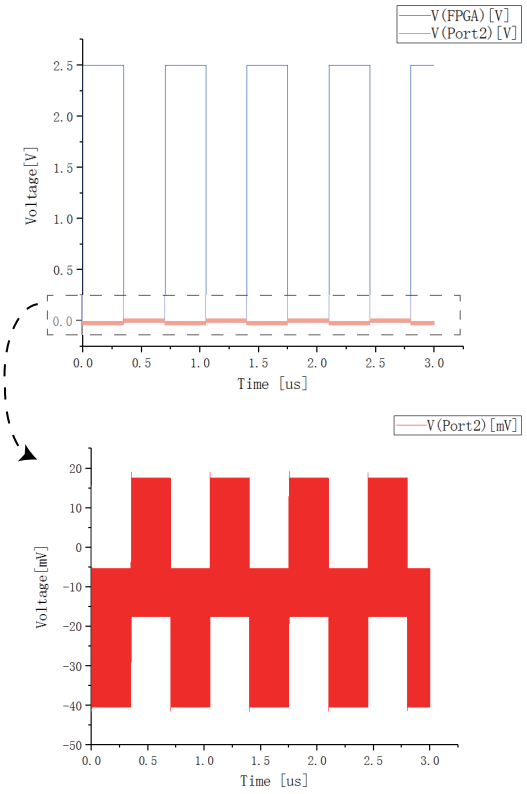

FIGURE 4. Envelope of amplitude modulation with the 50% duty cycle.

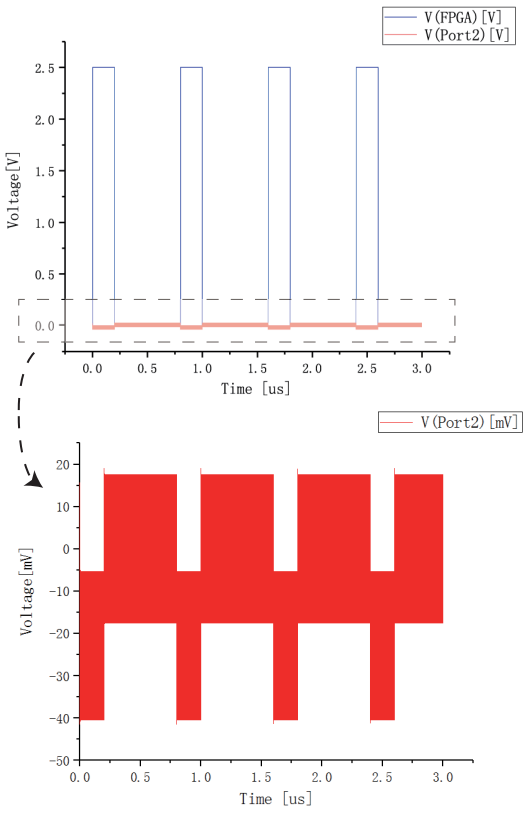

FIGURE 5. Comparison of envelopes of amplitude modulation with the 75% and 25% duty cycle.

amplitude modulation using the novel space-time MS structure, though their amplitudes are much less than the control voltage. It is worth noting that the above simulations are carried out by ANSYS Electronics Desktop 18.

Fig 6 (a) and Fig 6 (b) are the change of return loss and the phase, respectively. Given the MS a pulse bias-voltage 2 V produced from the FPGA with the on-off diodes, the different performance of return losses and phases can be observed after the CW through the MS. Return losses change (red line and black line) almost 2 dB from 5.58 GHz to 5.94 GHz, while the phases (red line and blue line) are constant in the same range. Therefore, the structure proposed can be used for the form of amplitude modulation.

To figure out the underlying principle of the whole absorption of the proposed MS, a periodic array of multilayer metal-dielectric was used [29]. Fig 7 shows the surface current distribution for each element patch of the PIN diodes of the ON/OFF state by the simulation. When the diodes are OFF, the more reflection signal can be obtained due to the fact that the patches are isolated from the ground. The more penetration signal, by contrast, should be estimated because the patches are shorted to the ground with the ON diodes. From the Fig 6, we can see the frequency range is from 5.55 GHz to 5.94 GHz beyond. So the pentagon spiral structure is a broadband polarized antenna structure and surface current can be absorbed or emission according to different conditions, which the controlled voltage is high or low. The direction of polarization is the same as that of the spiral and the surface current will present the performance of emission at one part of the spiral structure in Fig 7.

III. RESULT AND DISCUSSIONS

A. DESIGN OF MS SCHEME

In the measurement, a signal generator is connected to Port1 as a transmitter and a scope is connected to Port2 as a receiver. Above analysis can be described as Fig 8, a far-field signal is generated from Port1, through the MS structure and toward Port2. We add the PWM wave from FPGA as the local signal to the MS with different duty cycles. It appears reflection, scattering and projection phenomenon around the MS.

In the near-field situation, the compact quasi-optical system is designed to get the far field microwave [30]. The lens diameter ratio f/D (≈ 1) is too small and thick lens are necessary. A near-field measurement scheme is shown in Fig 9, and various theoretical analysis are discussed in [31]. The MS position and size given by the Gaussian beam technique as follows

$$d_{02} = f\left[1 + \frac{(d_{01}/f)-1}{((d_{01}/f)-1)^2 + \left(\pi w_{01}^2/\lambda f\right)^2}\right] \quad (9)$$

$$w_{02} = \frac{w_{01}}{\sqrt{((d_{01}/f)-1)^2 + \left(\pi w_2^{01}/\lambda f\right)^2}} \quad (10)$$

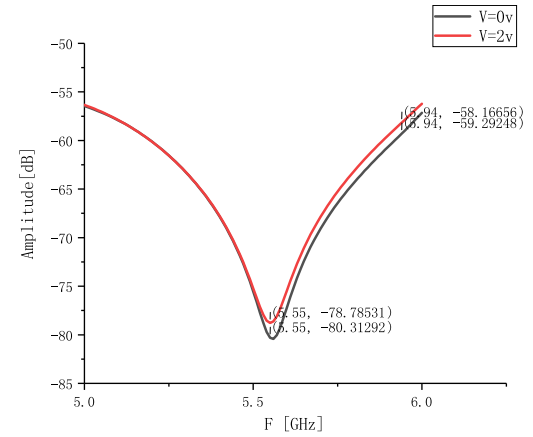

(a) The return loss

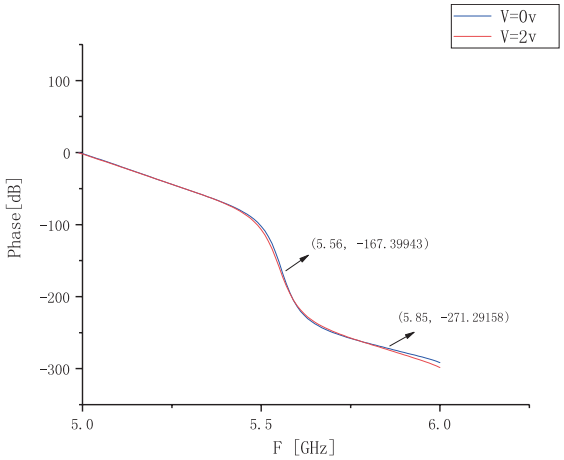

(b) Phase change

FIGURE 6. The return loss of (a)the amplitude component and (b) the phase component from 5 GHz to 6 GHz.

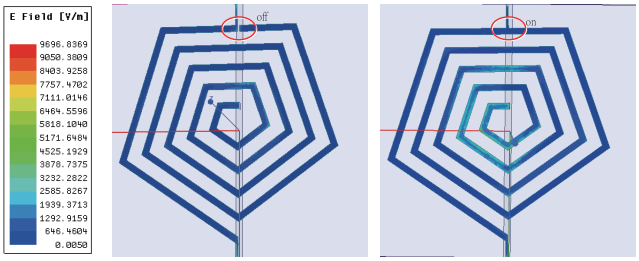

FIGURE 7. Simulation of the surface current distribution of each element with the ON/OFF states by ANSYS EM Desktop 18.

In the horizontal direction, d_1 is the distance from the input antenna1 to the lens, d_2 denotes the length between the lens and the MS, and d_3 presents the the width from MS to the output antenna2. In the vertical direction, w_{01} and w_{02} are the radius of input beam and the output beam, respectively.

Based on this design, a digital MS prototype from transmitter side is fabricated. Each digital element is made of a pentagon spiral metal patch printed on a ROGERS RO4003C substrate with a dielectric constant of 3.55, loss tangent

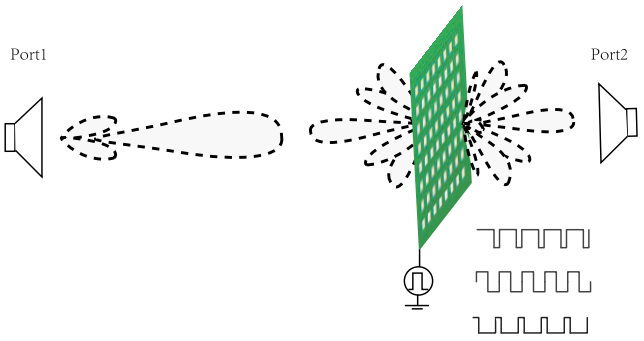

FIGURE 8. Reflection, scattering and projection phenomenon around the MS providing a PMW-based EM wave transmitted from the Port1 to the Port2 by FPGA.

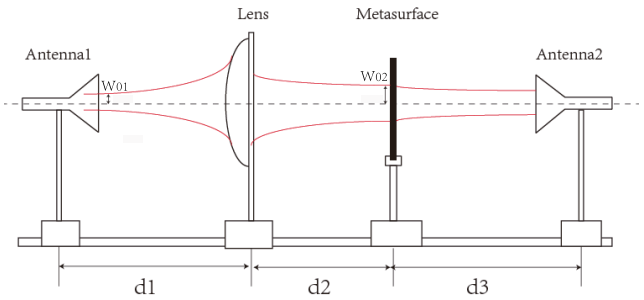

FIGURE 9. The setup of the simulations based on a quasi optical scheme. The lens is located between antenna1 and the MS.

of 0.0027, and thickness of 0.762 mm. The top layer of the structure consists of six columns with six connected elements, and the bottom of it is eight parallel lines connected together at up and down ends, and has an overall size of 137.16 mm * 137.16 mm. A SMA socket is set on the side, whose power end connected to the top board and the ground end connected to the bottom board. The pin diode connected between the input line and the spiral line in each element and its on-off status is controlled by the digital high-low voltage from FPGA device.

The measurements are carried out on a measurable scale shown in Fig 10. On one side of the scale, a linearly polarized horn antenna serves as the excitation source and it is connected to a signal generator (Rohde&Schwarz SMR), which provides the microwave signal at 5.85 GHz frequency. Another linearly polarized horn antenna receives the microwave signal via an oscilloscope (Agilent DSO81204B), which is set on the other side of the scale. In Fig 9, a thick lens with absorbing medium is located beside the antenna1, and the MS equipment under test (EUT) is mounted on a turnable shelf between the thick lens and the antenna2. $d1$, $d2$ and $d3$ are 30.3 cm, 9.4 cm and 23.8 cm respectively. FPGA hardware board (DE1-SoC) is connected to the SMA socket of the MUT, exploited to provide a 50% duty cycle on-off digital signal with 2.5 V control voltage. The FPGA is directly added on the test unit, in which a sequence is preloaded to generate six control voltages. The modulation period T_0 is 320 ns and the pulse width $T_{ioff} - T_{ion}$ is 160 ns, which corresponds to the

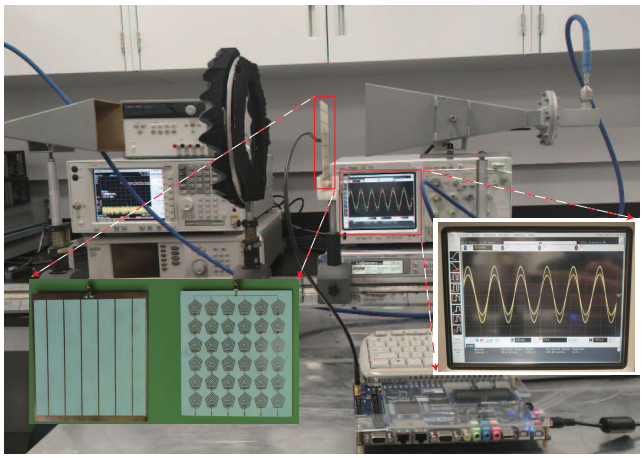

FIGURE 10. Prototype testing experiments when the unit time interval is 100 *ps*.

modulation frequency $f_0 = 31.25\ MHz$, and diode (MADP-000907) switch speed of 62.5 MHz, respectively. The output result of the oscilloscope can be seen in Fig 10. We can observe that the amplitude change obviously according to on-off voltage by holding the fixed phase component. The amplitude modulation is obtained as a good feature of the space-time MS to be used in wireless communication systems. According to the above analysis, the time scale can be changed to 1 us shown in Fig 11, the envelope can be seen in the oscilloscope.

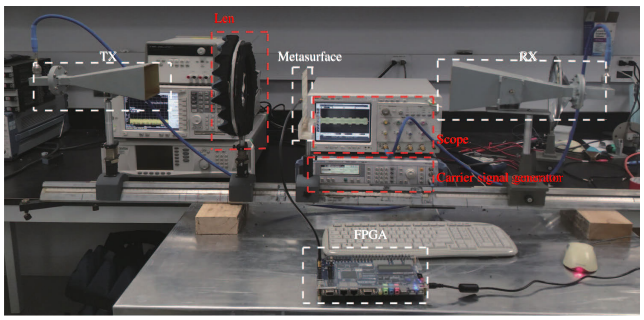

FIGURE 11. Prototype testing experiments when the unit time interval is 200 *ns*.

The output signal is an uniform amplitude waveform in Fig 12 (a) when the FPGA board is turned off. The measurements of 50 % duty cycle on-off digital signal from the FPGA can be observed in Fig 12 (b). The modulated envelope can be detected in Fig 12 (c) and Fig 12 (d) after the digital signal is modulated on the carrier signal directly using the proposed MS structure. Fig 12 (c) is observed provided that the parameters d1, d2 and d3 are setup at 30.3 cm, 9.4 cm and 23.8 cm, respectively. While Fig 12 (d) is shown when the parameters d1, d2 and d3 change to 27.3 cm, 12.4 cm and 23.8 cm, respectively. In addition, we can find that the debugging will change the propagation path of wave and affect the received energy eventually.

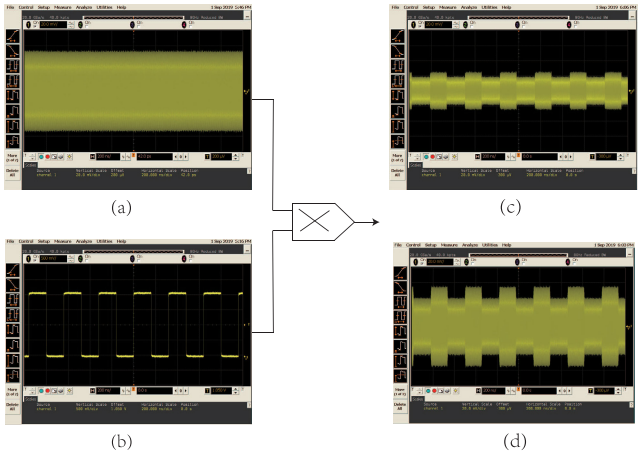

FIGURE 12. The measurements related to the simulations in Fig 4.

The horn antenna of the receiver side is connected to the spectrum analyzer, we can observe that the spectrum is spread around the transmit tone frequency 5.85 GHz in Fig 13, which is the performance of harmonic signal from programmable MS.

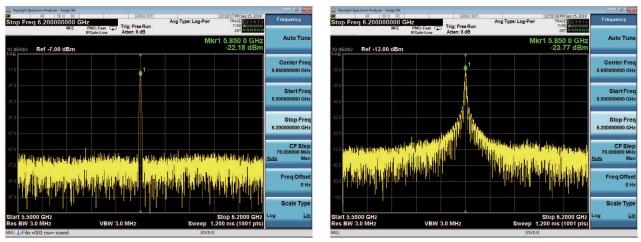

FIGURE 13. The performance of spread spectrum. Left is before time-varying programmable MS and right is after that.

IV. CONCLUSION

In this paper, we proposed a new architecture of the space-time MS to obtain an amplitude-based modulation scheme for fitting the requirements of wireless communication system. The architecture is successful fabricated and a quasi-optical scheme is designed to obtain the desired form of amplitude-based modulation. It is notice that software-defined pin diode ON / OFF switches are sufficient to build MSs for supporting an impressive range of EM functions. The proposed time-varying digital MS can be operated as a programmable modulation scheme, which can be used in wireless communication system. The results from both the simulations and measurements confirm the feasibility and reliability of the proposed scheme.

REFERENCES

[1] B. Zhang, J. Hendrickson, N. Nader, H.-T. Chen, and J. Guo, "Metasurface optical antireflection coating," *Appl. Phys. Lett.*, vol. 105, no. 24, Dec. 2014, Art. no. 241113.

[2] J. Hu, G. Q. Luo, and Z.-C. Hao, "A wideband quad-polarization reconfigurable metasurface antenna," *IEEE Access*, vol. 6, pp. 6130–6137, 2018.

[3] J. Valentine, S. Zhang, T. Zentgraf, E. Ulin-Avila, D. A. Genov, G. Bartal, and X. Zhang, "Three-dimensional optical metamaterial with a negative refractive index," *Nature*, vol. 455, no. 7211, pp. 376–379, Sep. 2008.

[4] Y. Yifat, M. Eitan, Z. Iluz, Y. Hanein, A. Boag, and J. Scheuer, "Highly efficient and broadband wide-angle holography using patch-dipole nanoantenna reflectarrays," *Nano Lett.*, vol. 14, no. 5, pp. 2485–2490, May 2014.

[5] G. Zheng, H. Mühlenbernd, M. Kenney, G. Li, T. Zentgraf, and S. Zhang, "Metasurface holograms reaching 80 percent efficiency," *Nature Nanotechnol.*, vol. 10, pp. 308–312, 2015.

[6] A. H. Safavi-Naeini, T. P. M. Alegre, M. E. J. Chan, Q. L. M. Winger, J. T. Hill, D. E. Chang, and O. Painter, "Electromagnetically induced transparency and slow light with optomechanics," *Nature*, vol. 472, pp. 69–73, Apr. 2011.

[7] L. Zhang, X. Q. Chen, S. Liu, Q. Zhang, J. Zhao, J. Y. Dai, G. D. Bai, X. Wan, Q. Cheng, and G. Castaldi, "Space-time-coding digital metasurfaces," *Nature Commun.*, vol. 9, no. 1, p. 4334, 2018.

[8] S. A. Stewart, T. J. Smy, and S. Gupta, "Finite-difference time-domain modeling of space–time-modulated metasurfaces," *IEEE Trans. Antennas Propag.*, vol. 66, no. 1, pp. 281–292, Jan. 2018.

[9] T. Hongnara, S. Chaimool, P. Akkaraekthalin, and Y. Zhao, "Design of compact beam-steering antennas using a metasurface formed by uniform square rings," *IEEE Access*, vol. 6, pp. 9420–9429, 2018.

[10] F. Costa, A. Monorchio, and G. Manara, "An overview of equivalent circuit modeling techniques of frequency selective surfaces and metasurfaces," *Appl. Comput. Electromagn. Soc. J.*, vol. 29, no. 12, pp. 960–976, Dec. 2014.

[11] S. N. Burokur, J.-P. Daniel, P. Ratajczak, and A. de Lustrac, "Tunable bilayered metasurface for frequency reconfigurable directive emissions," *Appl. Phys. Lett.*, vol. 97, no. 6, Aug. 2010, Art. no. 064101.

[12] S. Lim, C. Caloz, and T. Itoh, "Metamaterial-based electronically controlled transmission-line structure as a novel leaky-wave antenna with tunable radiation angle and beamwidth," *IEEE Trans. Microw. Theory Techn.*, vol. 53, no. 1, pp. 161–173, Jan. 2005.

[13] K. Achouri and C. Caloz, "Design, concepts, and applications of electromagnetic metasurfaces," *Nanophotonics*, vol. 7, no. 6, pp. 1095–1116, Jun. 2018.

[14] S. H. Lee, M. Choi, T.-T. Kim, S. Lee, M. Liu, X. Yin, H. K. Choi, S. S. Lee, C.-G. Choi, S.-Y. Choi, X. Zhang, and B. Min, "Switching terahertz waves with gate-controlled active graphene metamaterials," *Nature Mater.*, vol. 11, no. 11, pp. 936–941, Nov. 2012.

[15] Y. Hadad, D. L. Sounas, and A. Alu, "Space-time gradient metasurfaces," *Phys. Rev. B, Condens. Matter*, vol. 92, no. 10, Sep. 2015, Art. no. 100304.

[16] S.-F. Shi, B. Zeng, H.-L. Han, X. Hong, H.-Z. Tsai, H. S. Jung, A. Zettl, M. F. Crommie, and F. Wang, "Optimizing broadband terahertz modulation with hybrid graphene/metasurface structures," *Nano Lett.*, vol. 15, no. 1, pp. 372–377, Jan. 2015.

[17] Q. Wang, X. Zhang, Y. Xu, J. Gu, Y. Li, Z. Tian, R. Singh, S. Zhang, J. Han, and W. Zhang, "Broadband metasurface holograms: Toward complete phase and amplitude engineering," *Sci. Rep.*, vol. 6, no. 1, p. 32867, Dec. 2016.

[18] X. Ni, A. V. Kildishev, and V. M. Shalaev, "Metasurface holograms for visible light," *Nature Commun.*, vol. 4, no. 1, p. 2807, Dec. 2013.

[19] G. Minatti, M. Faenzi, E. Martini, F. Caminita, P. De Vita, D. Gonzalez-Ovejero, M. Sabbadini, and S. Maci, "Modulated metasurface antennas for space: Synthesis, analysis and realizations," *IEEE Trans. Antennas Propag.*, vol. 63, no. 4, pp. 1288–1300, Apr. 2015.

[20] S. Pandi, C. A. Balanis, and C. R. Birtcher, "Design of scalar impedance holographic metasurfaces for antenna beam formation with desired polarization," *IEEE Trans. Antennas Propag.*, vol. 63, no. 7, pp. 3016–3024, Jul. 2015.

[21] D. Wang, L. Zhang, Y. Gu, M. Q. Mehmood, Y. Gong, A. Srivastava, L. Jian, T. Venkatesan, C.-W. Qiu, and M. Hong, "Switchable ultrathin quarter-wave plate in terahertz using active phase-change metasurface," *Sci. Rep.*, vol. 5, no. 1, p. 15020, Dec. 2015.

[22] C. H. Chu, M. L. Tseng, J. Chen, P. C. Wu, Y.-H. Chen, H.-C. Wang, T.-Y. Chen, W. T. Hsieh, H. J. Wu, G. Sun, and D. P. Tsai, "Active dielectric metasurface based on phase-change medium," *Laser Photon. Rev.*, vol. 10, no. 6, pp. 986–994, Nov. 2016.

[23] J. Zhao and Y. Cheng, "Ultrabroadband microwave metamaterial absorber based on electric SRR loaded with lumped resistors," *J. Electron. Mater.*, vol. 45, no. 10, pp. 5033–5039, Oct. 2016.

[24] J. Luo and T. J. Cui, "2-bit ultrathin amplitude-modulated coding metasurfaces with inserted chip resistors," in *Proc. IEEE Int. Conf. Comput. Electromagn. (ICCEM)*, Mar. 2019, pp. 1–3.

[25] Y. Wang and A. Tennant, "Experimental time-modulated reflector array," *IEEE Trans. Antennas Propag.*, vol. 62, no. 12, pp. 6533–6536, Dec. 2014.

[26] W. Yao and Y. Wang, "Direct antenna modulation—A promise for ultra-wideband (UWB) transmitting," in *IEEE MTT-S Int. Microw. Symp. Dig.*, 2004, pp. 1273–1276.

[27] M. Salehi, M. Manteghi, S.-Y. Suh, S. Sajuyigbe, and H. G. Skinner, "A wideband frequency-shift keying modulation technique using transient state of a small antenna," *Prog. Electromagn. Res.*, vol. 143, pp. 421–445, Nov. 2013.

[28] L. Chen, R. Zheng, Y. Zhou, W. Zhang, and R. Yan, "Research on optimization of LMS frequency estimation based on FPGA technology," in *Proc. Int. Conf. Smart Veh. Technol., Transp., Commun. Appl.*, 2018, pp. 25–32.

[29] F. Ding, Y. Cui, X. Ge, Y. Jin, and S. He, "Ultra-broadband microwave metamaterial absorber," *Appl. Phys. Lett.*, vol. 100, no. 10, Mar. 2012, Art. no. 103506.

[30] P. F. Goldsmith, "Quasi-optical techniques," *Proc. IEEE*, vol. 15, no. 11, pp. 372–377, Nov. 2019.

[31] J. Tuovinen, T. M. Hirvonen, and A. V. Raisanen, "Near-field analysis of a thick lens and horn combination: Theory and measurements," *IEEE Trans. Antennas Propag.*, vol. 40, no. 6, pp. 613–619, Jun. 1992.

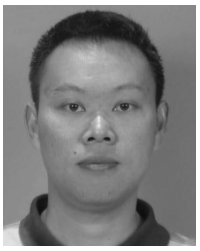

LIWEN CHEN (Member, IEEE) received the Ph.D. degree in communication and information systems from Wuhan University, China, in 2016.

He was a Postdoctoral Research Fellow of the Department of Electrical Engineering, Polytechnique de Montréal, Canada, from 2018 to 2019. In August 2003, he joined the Fujian University of Technology, where he is an Associate Professor and a master's degree Supervisor with the Department of Electronic Science and Technology. He has authored over 30 conference and journal articles. He was supported by ten funding projects. He holds 20 patents. His research interests include all fields of theoretical, computational, and technological EM, including novel MS, GNSS navigation and position applications, exotic antenna systems, and real-time radios. He received several awards, including the Wuhan University Outstanding Class Leader three times, from 2014 to 2016, the Wuhan University Academic Innovation Award, in 2015, the Wuhan University Second Class Scholarship, in 2015, and the Wuhan University First Class Scholarship, in 2016.

QING WENG received the B.Eng. and M.Eng. degrees from Fuzhou University, China, in 2003 and 2008, respectively. She worked as an RF Design Engineer, from 2008 to 2010. In 2011, she became a patent engineer. She is currently a Research Associate with the Fujian University of Technology. Her initial research focuses on localized waves with applications in the design of antennas. Her current research interests include optoelectronic devices, surface plasmonic effects, and analog signal processing for millimeter-wave systems.

JING CHEN received the B.Eng. and M.Eng. degrees from Fuzhou University, China, in 2005 and 2008, respectively. She is currently a Lecturer with the Fujian University of Technology and has participated in the research and development of many scientific research projects. Her research interests include designing embedded systems, microwave communication systems, and EM engineering.

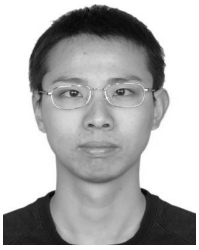

JIAN-FENG GU (Member, IEEE) received the B.E. degree from Northeast University, Shenyang, China, in 1999, the M.E. and Ph.D. degrees from the University of Electronic Science and Technology of China (UESTC), Chengdu, China, in 2004 and 2008, respectively, and the Ph.D. degree from Concordia University, Montréal, QC, Canada, in 2013, all in electrical engineering.

He was a Postdoctoral Fellow of the UESTC, from 2008 to 2010, and the Polytechnique de Montréal, from 2013 to 2016. He was the Director of algorithms at Zhuhai Naruida Ltd., China, from 2016 to 2017. From November 2017 to September 2019, he was a Research Associate with the Polytechnique de Montréal. From September 2019 to November 2019, he was a Research Associate with the École de Technologie Supérieure (ETS), Quebec University, QC, Canada. He is currently the Chief Scientific Officer (CSO) of Moonshot Health, Montréal. He has authored or coauthored more than 40 refereed articles and holds a number of patents. His research interests include advanced signal processing techniques for communication and radar systems, high-resolution spectral analysis and array processing, adaptive filtering, multiple targets localization and tracking, and knowledge-based signal processing as well as radar systems for medical and healthcare applications.